ELSEVIER

Polymer 40 (1999) 4685–4694

polymer

The effect of solid wall interaction on an amorphous polyethylene thin film, using a Monte Carlo simulation on a high coordination lattice

J.H. Jang, W.L. Mattice*

The Maurice Morton Institute of Polymer Science, University of Akron, Akron, OH 44325-3909, USA

Dedicated to Professor Ronald K. Eby on the occasion of his 70th birthday

Received 14 July 1998; received in revised form 11 January 1999; accepted 17 January 1999

Abstract

A Monte Carlo simulation on a high coordination lattice employing the RIS scheme for short-range interaction and a Lennard–Jones potential for long-range interaction was carried out on C_{120} polyethylene thin film adsorbed at an impenetrable solid wall as well as free-standing films at 443 and 343 K, respectively. The interaction between the solid wall and polymer chains was given by a step-like function whose well depth is ϵ. Three ϵ values, -6.0, -2.0, and 0.0 kJ/mol, were tested in order to study the influence of the solid wall on the static and dynamic properties of the film. Significant density increase near the solid wall with the strongest interaction was observed, giving rise to the contraction of film thickness, which is in accordance with experimental observation. The presence of the solid wall reduces the interfacial width relative to the free-standing film and the extent of the reduction shows a tendency to grow with the strength of the interaction and lowering temperature. The population of chain end groups is significantly depressed near the attractive solid wall. The chain mobility as a whole in the normal direction toward the film surface is retarded near the free surface and the solid wall, while the bead mobility is dependent on the nature of interactions.

Keywords: Solid wall interaction; Amorphous polyethylene thin film; Free standing film

1. Introduction

Three kinds of boundaries can be imposed on a polymer film; free surfaces on both sides, a free surface on one side with a solid boundary on the other, and solid walls at both sides. The case of one free surface with a solid boundary has attracted the most attention as it is ubiquitous in many practical applications such as adhesion and coating. It is generally believed that increased chain mobility near the free surface regions and conversely, decreased chain mobility near a solid surface, make the chain properties in a thin film differ from those of the bulk. The overall properties of a film, however, would not be affected when the film becomes too thick to be perturbed by its boundaries.

Much of the deviation from bulk properties comes out along the direction normal to the surface of a thin film. There have been many experimental efforts to observe the change of properties of the thin film, which includes a significant change in chain mobility near a solid surface [1], increase and/or decrease of the glass transition temperature [2], change in thermal expansion [3,4], broader relaxation spectrum compared to that of the bulk [5], chain end segregation in the surface region [6–8] and so on. It is quite obvious that the nature of the interactions at a polymer/solid surface and polymer/free surface becomes important in a thin film. The dramatic influence of the interaction on properties has been shown in the totally different behaviors of glass transition temperature, increase [3] and decrease [9], of polystyrene thin film on a hydrogen-terminated silicon surface and silicon native-oxide surface, respectively. However, the detailed behavior upon changing the interaction at the molecular level has not been understood. Another important issue in a thin film supported on a solid surface is the length scale over which the effects of two different surfaces extend. In the molecular dynamics simulation of Mansfield and Theodorou [10], the interfacial thickness in the free surface region of atactic polypropylene was calculated to be roughly 7 Å based on the density profiles, which corresponded to the length scale of a few monomer units. By the Brillouin light scattering study on a freely standing polystyrene thin film, Forrest et al. [11] found the interfacial width to be around the end-to-end distance of the chains in the sample. Frank et al. [1] observed retarded mobility in a series of thin films whose thickness is less than 1500 Å. They concluded the retardation results from the fixed contact of polymer chains to the solid surface, and the length

* Corresponding author. Fax: +1-330-9725396.

0032-3861/99/$ - see front matter
PII: S0032-3861(99)00071-3

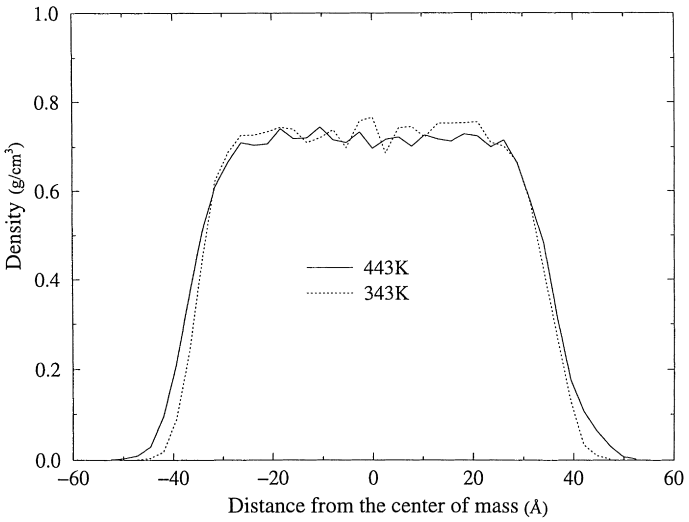

Fig. 1. The density profiles of the freely standing amorphous polyethylene thin films of 40 chains of C_{120} at 443 K (solid line) and 343 K (dotted line) in the direction normal to the surface.

scale up to the contour length of the polymer chain would be affected by the solid surface. Hu and Granick [12] observed the effect of the solid surface could extend up to 5 or $6R_g$ length scale, where R_g denotes the radius of gyration. Recently, Lin et al. [13] showed the effective range of the attractive solid wall on the interdiffusion process is between 300 and 400 Å, or 3 and $4R_g$. From these observations, it is generally expected that the effective range of a free surface is related to the dimension of the single chain. A solid wall produces a more complicated situation, with dependence on the nature of the interaction between the solid wall and chain molecules.

In this study, a lattice Monte Carlo simulation was used to understand the details of the chain dynamics in a thin film of amorphous polyethylene upon changing the short-range interaction between the polymer and a structureless solid wall from simple exclusion to attraction. The lattice version of the molecular system used in this simulation represented a monodisperse polyethylene film composed of 40 chains of linear $C_{120}H_{242}$. The size of each chain is not large enough to possess complete entanglement. The simulation technique has proven to be quite successful to visit specific questions of long time scale behavior without losing molecular details in the areas of self diffusion of polyethylene melts [14] and cohesion between two polymer melts [15].

2. Computational details

2.1. Bulk structure

The bulk structure of an amorphous C_{120} was prepared for use in generation of the model of the thin film. The monodisperse melt of 40 chains of C_{120} was mapped onto the periodic second nearest neighbor diamond (2nd) lattice whose *xyz* dimension was 23 × 21 × 27, in units of the step length, 2.5 Å, on this lattice. The density is 0.72 g/cm^3. The 2nd lattice is produced by discarding every 2nd lattice in the diamond lattice. As our lattice employs a coarse-grained version of each ethylene monomer, this mapping generated 60 beads for each C_{120} chain. This lattice has a coordination number of 12, and is identical with the hexagonal closest packing of uniform hard spheres. The coarse-grained structure, high coordination, and a specially devised energetics have provided a great deal of efficiency in simulating polymer properties without losing molecular detail [14–17]. In this simulation, one Monte Carlo step is defined as the simulation length when every bead has attempted one move, on an average.

The single bead move was performed with the restriction of a self-avoiding random walk, so that a chain on the 2nd lattice cannot pass through itself [18]. Additional terms in the Hamiltonian control the short-range [19] and long-range [20] interactions. The initial structure was relaxed at 443 K using two million steps of Monte Carlo simulation, employing only RIS [21] potential scheme for the Metropolis algorithm. Further relaxation was achieved with five million steps of Monte Carlo simulation employing both the RIS potential and long-range interactions obtained from the lattice description of the Lennard–Jones potential. The energetics used in this simulation has been described in detail elsewhere [18–20,22].

2.2. Freely standing film

The expansion of the periodic boundary condition along one direction (*z*) of an amorphous cell is a successful way to generate a freely standing thin film in molecular dynamics [23] and Monte Carlo simulations [17]. The thin film structure of C_{120} was generated by the expansion of the periodicity along the *z*-direction to 120 units, followed by another ten million Monte Carlo steps of relaxation at 443 K, with

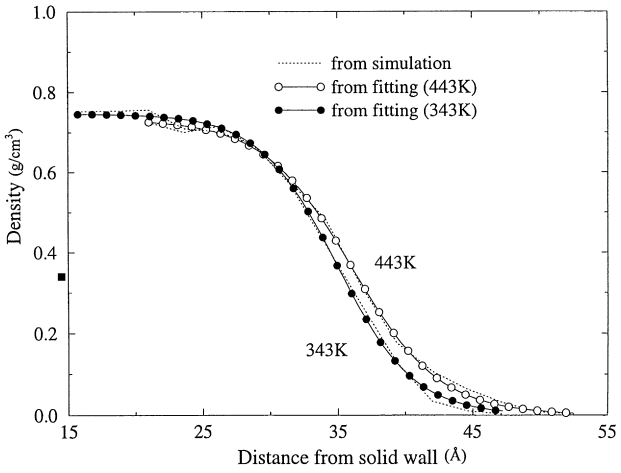

Fig. 2. The fitting of interfacial profiles of freely standing films at 443 K (open circle) and 343 K (filled circle) to Eq. (2).

the same short-range and long-range interactions as in the bulk case. Equilibrium was confirmed by the total energy fluctuation during the simulation. The final equilibriated structure at 443 K was chosen to be the starting geometry for the simulation at 343 K. At this temperature, ten million steps of Monte Carlo simulation was done for relaxation and equilibriation.

2.3. Solid substrate

The solid substrate was incorporated by introducing an external bead-wall interaction term. The solid substrate was located at $z = 0$ of the final structures obtained from the freely standing film generation. Beads were not allowed to move from $z = 0$ to -1, which means the substrate was considered as an impenetrable wall. The adsorption sites located at the wall come from the same lattice geometry as that of the 2nd lattice in the *xy*-dimension. The total number of available sites is 23×21. A step-like external function whose well depth is ϵ was applied to all the beads in the layer with $z = 0$. Three cases of $\epsilon = -6.0$, -2.0, and 0.0 kJ/mol were used in this simulation. Hereafter, strong interaction, medium interaction and non-interaction will refer to aforementioned interactions. Then, the total energetics during the trial of a bead for move in this simulation can be expressed by

$$\Delta E_{ij} = \Delta E(\text{RIS})_{ij} + \Delta E(\text{long-range})_{ij} + \Delta E(\text{bead-wall})_{ij}. \quad (1)$$

The simulations were done at two temperatures, 443 and 343 K, for ten million Monte Carlo steps with the Metropolis algorithm with all the three energy terms in Eq. (1).

Table 1
The optimized parameters from the curve fitting using Eq. (2) for the density profiles of the freely standing films at 443 and 343 K

	h (Å)	w (Å)	ϕ_{bulk} (g/cm^3)
443 K			
Free-standing[a]	35.97 ± 0.17	12.97 ± 0.54	0.732 ± 0.009
0.0 kJ/mol	84.88 ± 0.10	12.28 ± 0.33	0.746 ± 0.004
− 2.0 kJ/mol	84.40 ± 0.12	12.15 ± 0.40	0.741 ± 0.005
− 6.0 kJ/mol	71.16 ± 0.09	11.30 ± 0.32	0.742 ± 0.004
343 K			
Free-standing[a]	34.86 ± 0.15	11.36 ± 0.52	0.746 ± 0.007
0.0 kJ/mol	83.90 ± 0.40	9.40 ± 1.54	0.762 ± 0.017
− 2.0 kJ/mol	83.79 ± 0.16	9.29 ± 0.63	0.771 ± 0.007
− 6.0 kJ/mol	83.75 ± 0.16	6.04 ± 0.56	0.741 ± 0.008

[a] For the freely standing film, the position of $z = 0$ is defined as the center of mass of the film.

3. Results and discussion

3.1. Bead density profiles

Fig. 1 shows the bead density profile for freely standing films at 443 and 343 K. At 343 K, a small contraction of film thickness compared to 443 K produced a stiffer interfacial density profile and an increase of density in the middle of film. The free surface regions were fitted to the following analytical function [24].

$$\phi(z) = \phi_{\text{bulk}}\{1 - \tanh[2(z - h)/w]\}/2 \quad (2)$$

where ϕ is the density, z the direction normal to the film surface, h the location of the interface, and w the interfacial width. Three variables, ϕ_{bulk}, h, and w, were used for the fitting parameters. As shown in Fig. 2, the fitting with Eq. (2) to the interfacial profiles at both temperatures is adequate, giving χ^2 values less than 0.001 Table 1 contains the optimized parameters obtained from the fitting for the freely standing films and the solid supported films at both temperatures. From the h and ϕ_{bulk} values, the freely standing film at 443 K was found to have 3.3% expansion in the film thickness and 1.9% decrease in the bulk density compared to the film at 343 K. If the average densities are taken from the $z = -20.0$ to $+20.0$ Å in Fig. 1, the bulk densities are 0.736 ± 0.021 and 0.720 ± 0.012 g/cm^3 for 343 and 443 K respectively, giving a 2.3% decrease in the bulk density as the temperature rises from 343 to 443 K. The difference in the densities at 343 and 443 K is comparable with the standard deviation in the estimate of the density, which implies a large uncertainty in an estimate of the thermal expansion coefficient. However, it is worthwhile to note the approximate size of the thermal expansion coefficients deduced from the estimate. The thermal expansion coefficient was calculated to be 1.9×10^{-4}/deg based on the ϕ_{bulk} of the fitting and 2.3×10^{-4}/deg from the average density in the middle of the film. Both values are in the range of experimental values [25] for liquid state and solid state, which are 5.313×10^{-4}/deg and 2.013×10^{-4}/deg, respectively.

Fig. 3(a) depicts the bead density profiles of the films supported by the impenetrable walls with $\epsilon = -6.0$, -2.0, and 0.0 kJ/mol attractive potentials between the solid walls and beads at 443 K. From the inset of Fig.

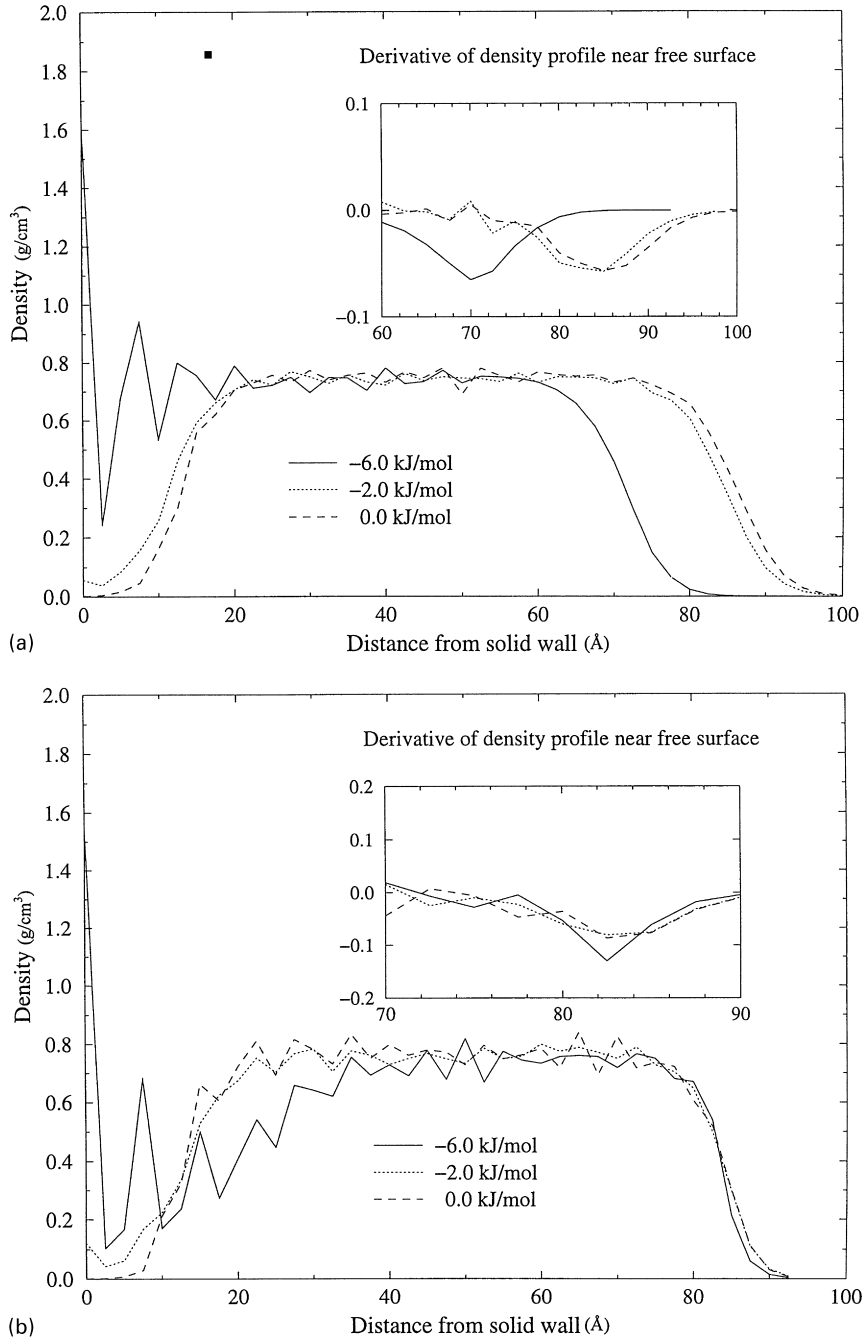

Fig. 3. (a) The density profiles of polyethylene thin films supported by a solid wall with interaction of − 6.0 kJ/mol (solid line), − 2.0 kJ/mol (dotted line), and 0.0 kJ/mol (dashed line) at 443 K; (b) similar density profiles at 343 K. The insets in (a) and (b) show the derivatives of the density against the *z* coordinate. The minimum of each curve was used to define the film thickness.

3(a), the film thickness was obtained at the minimum derivative points of the interfacial profiles near the free surface. The thickness of the film for the strong, medium, and weak interactions was found to be 71.0 ± 0.5, 82.9 ± 1.0, and 84.8 ± 1.0 Å, respectively. These values are quite similar to the optimized *h* values obtained from the fitting by Eq. (2), as shown in Table 1. This dependence of film thickness on the nature of the interaction can provide a basis in understanding the contradictory observations in the experimental works [3,9] on the glass transition behavior, which were done on polystyrene on hydrogen passivated silicon surface and polystyrene on oxidized silicon surface. Though our work does not give a direct information about the glass transition, it shows the importance of the interaction between polymer and solid surface on the film thickness. For the strong interaction case, a significant increase of density near the solid wall was observed, with an oscillatory damping pattern up to 30 Å. The oscillatory pattern in the

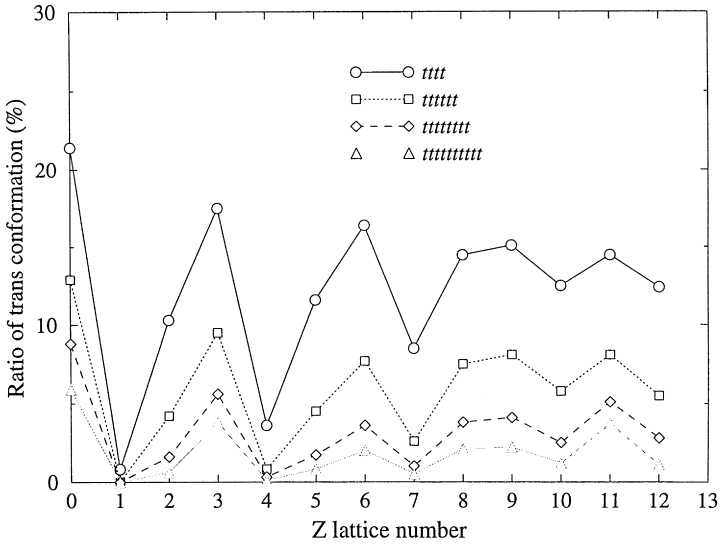

Fig. 4. The ratios of the bead occupied by the *tttt* (circle), *tttttt* (rectangle), *ttttttt* (diamond), and *ttttttttt* (triangle) local conformations to the total beads in the layers with strong interaction at 343 K against lattice number. The position of the solid wall is indicated by $z = 0$.

density profile in confinement or near a hard wall is quite common in lattice simulations [26]. This pattern can be attributed to the artificially flat surface of the hard wall and chain connectivity. The density increase in the strong interaction case leads to the decrease in the total film thickness compared to the thickness of a freely standing film. In contrast, the weaker interaction cases do not show the substantial increase of the density near the wall, because −2.0 kJ/mol gives only a slightly higher density than the 0.0 kJ/mol interaction. The density profiles for the weaker interaction cases are similar to that of the freely standing film, meaning that cohesive interaction between the chains is stronger than the weak attractions of the solid wall. This result implies that the weak interaction is a de-wetting situation as it does not provide a sufficient number of contacts with the solid surface. The adsorption energy per chain for the weak interaction at 443 K was calculated to be only 0.3 ± 0.3 kJ/mol, which is much smaller than that of the strong interaction case, 26.8 ± 0.7 kJ/mol.

The interfacial density profiles near the free surface in Fig. 3(a) are very similar, but the interfacial widths obtained from the curve fitting using Eq. (2), as shown by the values of w in Table 1, weakly depends on the interaction energy between the wall and beads. The interfacial widths of the films with solid wall are always smaller than that of the free film and the favorable interaction results in a decrease of the interfacial width. It should be noted that there are other factors to affect the interfacial width, such as film thickness, system size, and surface tension in the presence of the capillary wave fluctuation [27–31]. In our study, the contribution cannot be separated because our concern focuses on the bead-wall interaction. Nevertheless, our findings qualitatively indicate that the interfacial width of the free film which probably contains the contribution of the thermal fluctuation largely decreases by the presence of a sold wall and the size of the effect depends on the strength of the applied potential between the wall and beads.

The same analysis of the films equilibrated at 343 K is plotted in Fig. 3(b). A dramatic change in density profile was observed for the strong interaction case. No significant contraction in the film thickness compared to other weaker interaction cases was observed. Instead there is a depletion region around 10–35 Å which is larger than that at 443 K. The bead density adsorbed onto the solid wall is similar to that at 443 K, which produces 25.9 ± 0.5 kJ/mol of adsorption energy per chain. Near the solid wall, higher density peaks were observed at every third lattice step (every 7.5 Å) with depletion layers between the higher density layers. This increased density at the wall as a result of the strongly favorable bead-wall interaction leads to a depletion of density in the adjacent layer because of the repulsive long-range interaction between two neighboring beads separated only by 2.5 Å. The highly extended local conformation running parallel to the solid wall was found at the peak positions. From Fig.4, the ratios of the beads occupied by the *tttt* local conformation to the total beads in the layers are 21.4, 17.5, 16.4, and 15.1% at $z = 0$, 3, 6, and 9, respectively, which is larger than in the other layers. Fig. 4 also shows the ratios corresponded to the *tttttt*, *ttttttt*, and *ttttttttt* local conformations. The extended local conformations are connected with each other within a layer and between layers. As the ratio of the extended conformation is lower in the bulk region of the film, crystallization of the whole film is not achieved at 343 K. Instead, sequences of bonds in the *trans* conformation are induced by the attractive surface in the higher density layers at the low temperature.

The interfacial widths at 343 K shown in Table 1 are always smaller than those at 443 K for the corresponding interactions, which implies that there exists an effect that the thermal fluctuation near the free interface is suppressed at

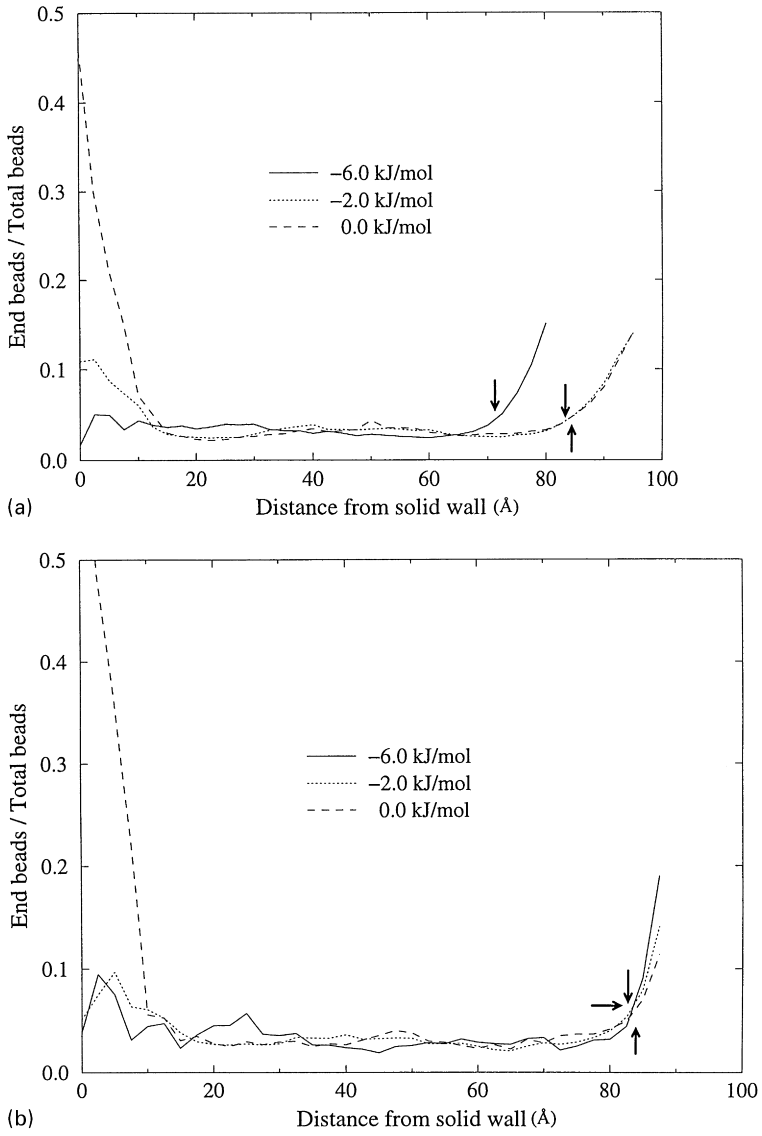

Fig. 5. (a) The distribution of chain ends for the polyethylene thin film supported by a solid wall with interaction of −6.0 kJ/mol (solid line), − 2.0 kJ/mol (dotted line), and 0.0 kJ/mol (dashed line) at 443 K; (b) the distribution of chain ends at 343 K. The distribution was calculated by dividing the number of end beads by the total number of beads at each z coordinate. Arrows indicate the chain ends distributions at the film thickness are obtained from the minimum derivative of the density profile.

the lower temperature. As at 443 K, the interfacial width decreases by introducing a solid wall and the extent of the decrease gets larger with the strength of the applied potential. Especially, the interfacial width for the strong attraction case at 343 K is much smaller than other cases, which indicates that the thermal fluctuation at the free interface can be greatly suppressed by the combination of the low temperature and the strongly favorable interaction with the solid wall.

3.2. End beads distribution

The distributions of end beads are shown in Fig. 5(a) and (b) for 443 and 343 K, respectively. The distribution was obtained by dividing the total number of end beads by the total number of beads at certain z layers. The value for the distribution in the bulk should be 2 (end beads)/60 (total beads) = 0.033. The somewhat higher values very near the free surface can be attributed to the known tendency for segregation [6–8] of chain ends at a free surface. When taken at the film thickness obtained from the derivatives shown in the insets of Fig. 3(a) and (b), the end beads distribution is in the range of 0.040–0.058, which is nearly twice the bulk value. The values are 0.041 ± 0.005, 0.040 ± 0.005, and 0.042 ± 0.004 for the strong, medium, and non-interacting cases, respectively, at 443 K. At 343 K, 0.044 ± 0.006, 0.058 ± 0.008, and 0.057 ± 0.007 were obtained for the end beads distribution for the strong, medium, and non-interacting cases. According to the neutron reflectivity study of Zhao et al. [6], the population of chain ends in the free

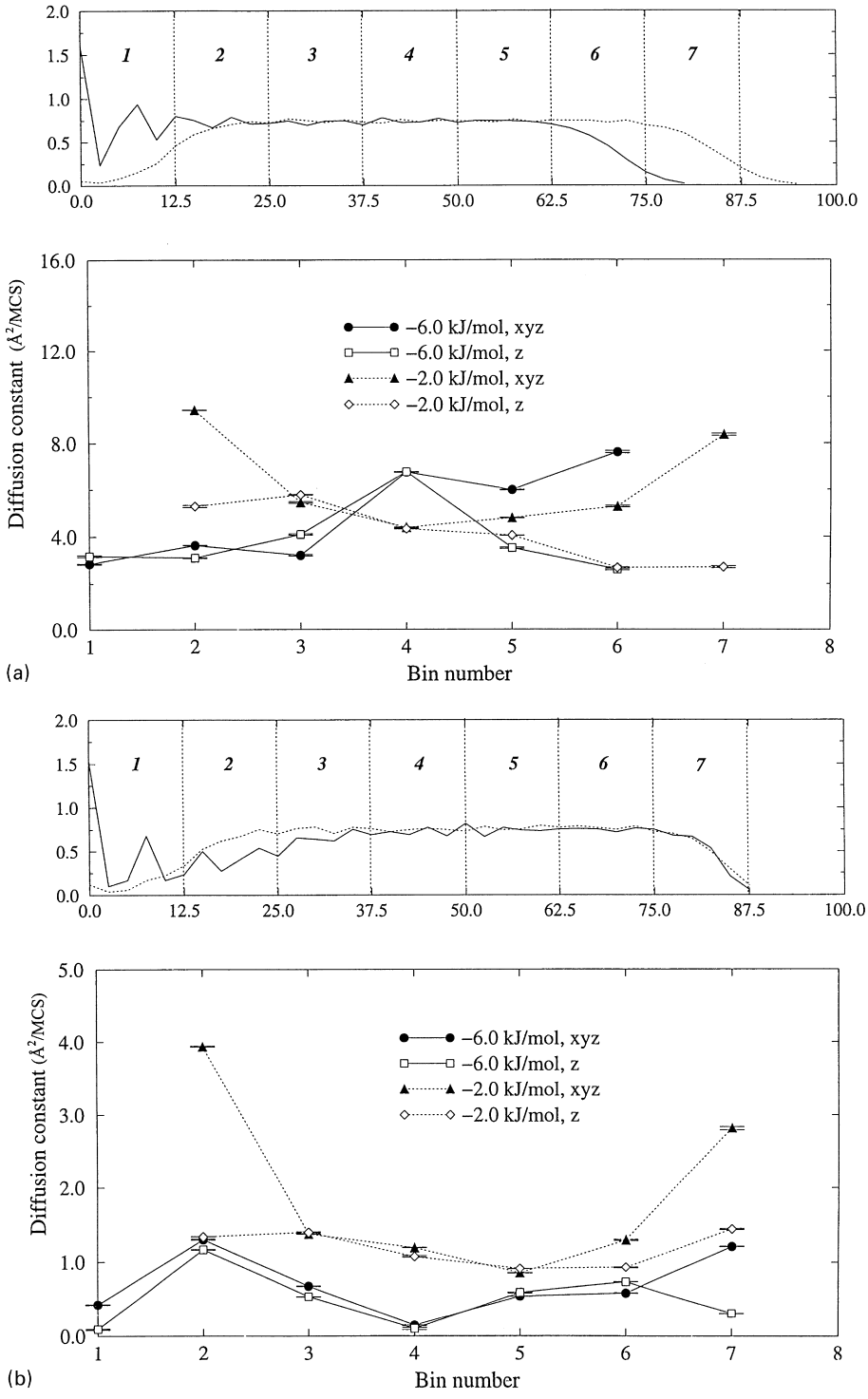

Fig. 6. (a) The center of mass diffusion constants in the *xyz* direction (filled) and along the *z* direction (open) normal to the film surface. The solid lines indicate the strong interaction (− 6.0 kJ/mol) and the dotted lines the weak interaction (− 2.0 kJ/mol). The top panel depicts how the entire film is divided into several bins.

surface region was found to be twice that of the bulk value. Therefore, our results are consistent with the experimental observation.

The end beads distribution near the solid wall is highly dependent on the nature of the interaction between the chain and the wall. In the case of strong interaction, no end beads enrichment near the solid wall was found. However, very large enrichment of end beads, which is even larger than that in the free surface region was observed for the non-interacting case. The existence of end beads at the solid

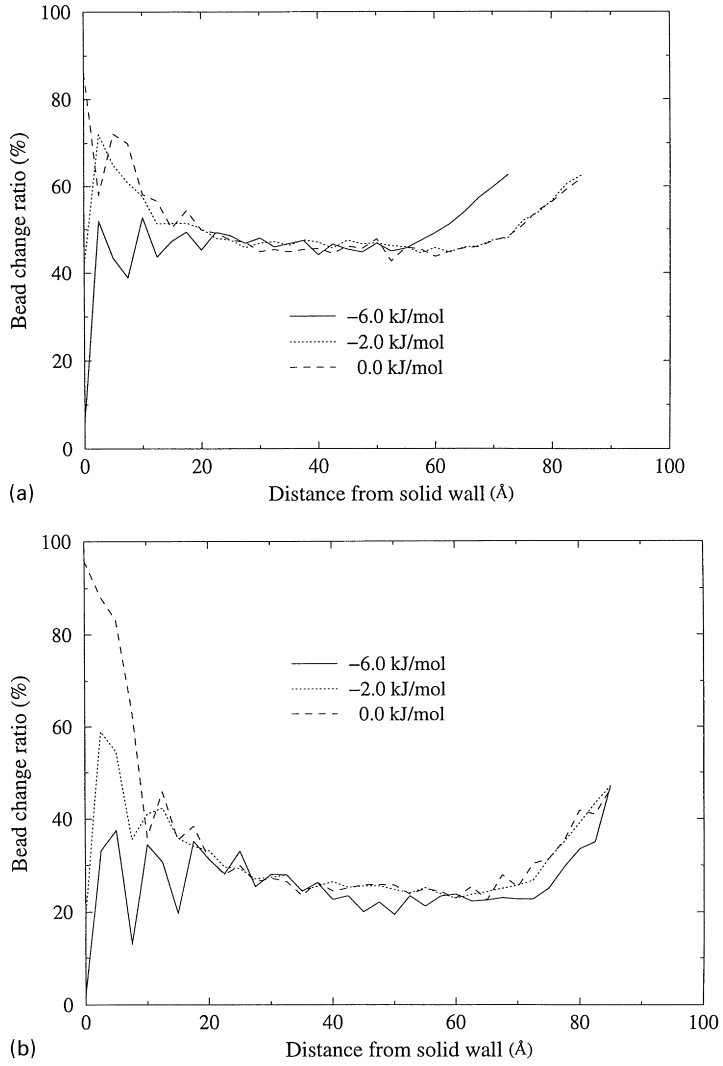

Fig. 7. (a) The bead flux profiles of the polyethylene thin film supported by solid wall with interaction of − 6.0 kJ/mol (solid line), − 2.0 kJ/mol (dotted line), and 0.0 kJ/mol (dashed line) at 443 K; (b) the similar bead flux profiles at 343 K. The value for the *y*-axis can be obtained by dividing the number of beads which changed the *z*-coordinate by the total number of beads at a *z* lattice coordinate in the sampling period, 2000 MCS.

wall does not provide the beads in the bulk region with full physical contact to the solid wall. If there is an enthalpy gain by the contact of any beads, which is the situation of the attractive interactions, then chain ends dislike the contact because the chain ends segregation reduces the total number of contacts. If there is an entropy loss by the contact, which is the case of the neutral solid wall as a result of confinement, then chain ends are more likely to locate at the wall, giving rise to a minimum number of total contact for all beads. Schaub et al. [7] did a neutron reflectivity experiment to study chain ends segregation on polystyrene with low-energy oligotetrafluoroethylene. Their main concern was the segregation in the free surface region, but their data show there is no significant chain end segregation near the silicon surface. Considering the favorable interaction between the silicon surface and fluoroethylene group, the chain end group segregation seems to be affected much more by the enthalpic effect than the entropic effect, which was also observed in this simulation.

3.3. Center of mass diffusion along with z direction

In order to see the chain mobility along with the *z* direction, the entire film was divided into several bins with 12.5 Å thickness which is similar to the size of the radius of gyration of C_{120} polyethylene single chain. The top panels of Fig. 6(a) and (b) show the division of the films for the 443 and 343 K cases. The overall center of mass diffusion constant, D_{xyz} (filled), and the *z* directional center of mass diffusion constant, D_z (open), were calculated in units of $Å^2$/MCS based on the following equations.

$$D_{xyz} = \frac{\sum_{i=0}^{N} \{r_{C.M.}(t+i) - r_{C.M.}(0+i)\}^2}{6t(N+1)}, \quad (3)$$

$$D_z = \frac{\sum_{i=0}^{N} \{z_{\mathrm{C.M.}}(t+i) - z_{\mathrm{C.M.}}(0+i)\}^2}{2t(N+1)}. \quad (4)$$

Here, N denotes the total number of conformations for the ensemble average. Two thousand conformations and four million Monte Carlo steps were used for N and t.

The diffusion constants are plotted for strong interaction (solid line) and medium interaction (dotted line) for chains with their center of mass originating in each bin as shown in the bottom panels of Fig. 6(a) and (b). As there is no reason to assume that the conversion between MCS and real time is independent of temperature, comparison should be restricted to diffusion coefficients at the same temperature, and should not extend to the comparison of diffusion coefficients at different temperatures.

The overall mobility near the strongly attractive solid wall is reduced to half that of the free surface region for 443 and 343 K. However, the medium interaction resulted in an increase of the overall center of mass diffusion constant near the solid wall at both temperatures and the diffusion constants are even larger than that in the free surface region. In a thermal equilibrium, -2.0 kJ/mol attractive interaction per site is not large enough to hold the beads at the wall against the cohesive interaction among the beads. There is more active dynamics near the wall with the medium interaction. The strong interaction can tightly hold of the beads at the solid wall, which produces a retarded mobility near the wall.

The chains with the centers of mass located initially in the bin number two in Fig. 6(b) showed an increased mobility at 343 K but did not for 443 K. According to the density profile in Fig. 3(b), there is a reduced density region near the solid wall. This reduced density provides more free volume leading to the increase of chain mobility.

In order to see the small scale movement of each bead along the z direction, a bead flux was calculated by checking out the change of the z lattice coordinate of each bead during the sampling period. The samples were taken at every 2000 MCS. As shown in Fig. 7(a) and (b), the bead movement in the free surface region is fairly mobile relative to the movement of the molecules as a whole. At 443 K, around 50% of the beads find new z positions while the value at 343 K is less than 30%. These values are increased to 62 and 45% in the free surface region at 443 and 343 K, respectively. The free surface regions for the increased bead mobility have a depth of about 20 Å, while the higher temperature gives a little bit longer scale than 343 K. The bead flux near the strongly attractive solid wall is almost similar to the bulk values showing an oscillatory pattern. However, with the weaker interaction, the bead can move back and forth along the z direction fairly freely even near the solid wall. This indicates that there exists a very active movement at a small scale near the weakly attractive solid wall, even though the large scale movement like the center of mass diffusion is greatly hampered.

4. Conclusions

The goal of this study is to provide an insight into how the interaction between the solid wall and polymer chains affects the static and dynamic properties of the film using a recently developed Monte Carlo simulation. Using the simulation tool, we were able to incorporate the energetics from the solid wall directly into our simulation.

1. There is a significant contraction of film thickness with a strongly favorable interaction in the equilibrium melt state (443 K). The contraction is mainly because of the bead adsorption onto the attractive solid wall. With the strongly favorable interaction, the contraction is not observed at 343 K, where higher density peaks appear repeatedly near the solid wall alternating with depletion layers. The layers corresponding to the higher density peaks contain extended local conformations running parallel to the solid surface. The runs of the *trans* conformation are connected to each other within a layer and between layers. It is attributed to the significance of single chain conformation induced by the attractive solid wall as the *gauche* state is not easily accessible near the attractive wall region at the low temperature.
2. The presence of the solid wall reduces the interfacial width compared to that of the free-standing film and the width decreases with the strength of the bead-wall interaction. At the lower temperature, the interfacial width is smaller than those at higher temperature with the same strength of the bead-wall interaction. One possible explanation is that there exists a broadening effect as a result of thermal fluctuation, which can be suppressed by the presence of the solid wall and by lowering the temperature.
3. The chain ends tend to locate at the neutral or weakly attractive wall as well as the free surface region. With the strongly attractive wall, we do not observe the chain ends segregation near the solid wall. The segregation would be affected by a small change of the interaction. This means that the chain ends segregation would have an enthalpic origin.
4. The mobility of chains along the z direction normal to a film surface is suppressed near the free surface and solid surface by the confinement effect, while overall diffusion tends to increase near a free surface and to decrease near attractive solid wall. However, the local mobility for each bead normal to the surface is more active in the free surface or weakly attractive wall than in the bulk state.
5. From the density profile and the local bead mobility, the length scale over which the effect of a free surface extends into the bulk region is around 20 Å, which is $\sim 2R_g$ scale. The free surface is affected by the presence of the solid wall, the strength of the bead-wall interaction, and temperature, even though the solid wall is located $6-7R_g$ far from the free surface in our simulation.

It should be noted that our simulation has employed the artificial step-like function for the bead-wall interaction. This employment has forced us not to compare our results to the experimental results directly. Therefore, further study will include the incorporation of more realistic energy terms.

Acknowledgements

The support of NSF (DMR-95-23278) for this work is gratefully acknowledged. J.J. thanks Korea Kumho Petrochemical Co. for allowing access to the computer facilities including the Cray supercomputer and the Power Challenger machines.

References

[1] Frank B, Gast AP, Russell TP, Brown HR, Hawker C. Macromolecules 1996;29:6531.
[2] Keddie JL, Jones RA, Corey RA. Faraday Discuss 1994;98:219.
[3] Wallace WE, van Zanten JH, Wu WL. Phys Rev E 1995;52:R3329.
[4] van Zanten JH, Wallace WE, Wu WL. Phys Rev E 1996;53:R2053.
[5] Hall DB, Hooker JC, Torkelson JM. Macromolecules 1997;30:667.
[6] Zhao W, Zhao X, Rafailovich MH, Composto RJ, Smith SD, Satkowski M, Russell TP, Dozier WD, Mansfield T. Macromolecules 1993;26:561.
[7] Schaub TF, Kellogg GJ, Mayes AM, Kulaskere R, Ankner JF, Kaiser H. Macromolecules 1996;29:3982.
[8] Kajiyama T, Tanaka K, Takahara A. Macromolecules 1997;30:280.
[9] Keddie JL, Jones RA, Corey RA. Europhys Lett 1994;27:59.
[10] Mansfield KF, Theodorou DN. Macromolecules 1991;24:6283.
[11] Forrest JA, Dalnoki-veress K, Stevens JR, Dutcher JR. Phys Rev Lett 1996;77:2002.
[12] Hu H-W, Granick S. Science 1992;258:1339.
[13] Lin EK, Wu WL, Satija SK. Macromolecules 1997;30:7224.
[14] Doruker P, Mattice WL. Macromolecules 1997;30:5520.
[15] Jang J, Mattice WL. Polym Commun 1999;40:1911.
[16] Doruker P, Mattice WLJ. Chem Phys 1996;104:8742.
[17] Doruker P, Mattice WL. Macromolecules 1998;31:1418.
[18] Rapold RF, Mattice WLJ. Chem Soc Faraday Trans. 1995;91:2435.
[19] Rapold RF, Mattice WL. Macromolecules 1996;29:2457.
[20] Cho J, Mattice WL. Macromolecules 1997;30:637.
[21] Mattice WL, Suter UW. Conformational theory of large molecules. The rotational isomeric state model in macromolecular systems. New York: Wiley, 1994.
[22] Baschnagel J, Binder K, Doruker P, Gusev AA, Hahn O, Kremer K, Mattice WL, Müller-Plathe F, Murat M, Paul W, Santos S, Suter UW, Tries V. Adv Polym Sci 1999; submitted.
[23] Misra S, Fleming PD, Mattice WL. J Comput-Aided Mater Des 1995;2:101.
[24] Cifra P, Nies E, Karasz FE. Macromolecules 1994;27:1166.
[25] Wrasidlo W. Thermal analysis of polymers. Advances in polymer science, 13. New York: Springer, 1974.
[26] Neelov IM, Borisov OV. Binder K. Macromol Theory Simul 1998;7:141.
[27] Semenov AN. Macromolecules 1994;27:2732.
[28] Kerle T, Klein J, Binder K. Phys Rev Lett 1996;77:1318.
[29] Werner A, Schmid F, Müller M, Binder K. J Chem Phys 1997;107:8175.
[30] Sferrazza M, Xiao C, Jones RA, Bucknall DG, Webster J, Penfold J. Phys Rev Lett 1997;78:3693.
[31] Tolan M, Seeck OH, Schlomka J-P, Press W, Wang J, Sinha SK, Li Z, Rafailovich MH, Sokolov J. Phys Rev Lett 1998;81:2731.